GEOLOGY | THE GEOLOGICAL SOCIETY OF AMERICA®

https://doi.org/10.1130/G48290.1

Manuscript received 13 August 2020
Revised manuscript received 8 November 2020
Manuscript accepted 17 November 2020

A new model for the growth of normal faults developed above pre-existing structures

Emma K. Bramham[1]*, Tim J. Wright[1], Douglas A. Paton[2] and David M. Hodgson[2]
[1]Centre for the Observation and Modelling of Earthquakes, Volcanoes and Tectonics (COMET), School of Earth and Environment, University of Leeds, Leeds LS2 9JT, UK
[2]School of Earth and Environment, University of Leeds, Leeds LS2 9JT, UK

ABSTRACT

Constraining the mechanisms of normal fault growth is essential for understanding extensional tectonics. Fault growth kinematics remain debated, mainly because the very earliest phase of deformation through recent syn-kinematic deposits is rarely documented. To understand how underlying structures influence surface faulting, we examined fault growth in a 10 ka magmatically resurfaced region of the Krafla fissure swarm, Iceland. We used a high-resolution (0.5 m) digital elevation model derived from airborne lidar to measure 775 fault profiles with lengths ranging from 0.015 to 2 km. For each fault, we measured the ratio of maximum vertical displacement to length (D_{max}/L) and any nondisplaced portions of the fault. We observe that many shorter faults (<200 m) retain fissure-like features, with no vertical displacement for substantial parts of their displacement profiles. Typically, longer faults (>200 m) are vertically displaced along most of their surface length and have D_{max}/L at the upper end of the global population for comparable lengths. We hypothesize that faults initiate at the surface as fissure-like fractures in resurfaced material as a result of flexural stresses caused by displacements on underlying faults. Faults then accrue vertical displacement following a constant-length model, and grow by dip and strike linkage or lengthening when they reach a bell-shaped displacement-length profile. This hybrid growth mechanism is repeated with deposition of each subsequent syn-kinematic layer, resulting in a remarkably wide distribution of D_{max}/L. Our results capture a specific early period in the fault slip-deposition cycle in a volcanic setting that may be applicable to fault growth in sedimentary basins.

INTRODUCTION

Two end-member models that explain strain distribution during the evolution of fault systems are (1) the isolated model, whereby faults increase in length with displacement accumulation (the ratio of maximum vertical displacement to length, D_{max}/L, remains approximately constant) and fault tips propagate and interact incrementally; and (2) the constant-length model, whereby faults reach their final lengths near instantaneously, and fault tips interact by linkage with increasing displacement accumulation (e.g., Walsh et al., 2002; Rotevatn et al., 2019). These end-member models and the associated global compilation of D_{max}-L data (e.g., Walsh and Watterson, 1988; Peacock and Sanderson, 1991; Cowie and Scholz, 1992; Schultz and Fossen, 2002; Walsh et al., 2002; Rotevatn et al., 2019) have been widely used to evaluate fault populations in different settings, including mid-ocean ridges, magmatic rift systems, and extensional sedimentary basins (Gupta et al., 1998; Bohnenstiehl and Kleinrock, 2000; Polun et al., 2018).

Testing these models is problematic because (1) global compilations combine multiple data sets from noncomparable settings, span several orders of magnitude of fault throw, and have significant scatter, therefore the models do not have distinct distributions within D_{max}-L plots; (2) the style of early-stage fault growth requires data from syn-kinematic packages that are hard to observe or reconstruct (e.g., Walsh et al., 2002); and (3) the models need not be mutually exclusive (Rotevatn et al., 2019).

In this study, we investigate fault growth in syn-kinematic deposits using data from the northern Krafla fissure swarm (KFS), Iceland, a region where an established fault system was near-instantaneously magmatically resurfaced by the Storaviti lava flow at ca. 10 ka (Sæmundsson, 1991; Jóhannesson and Sæmundsson, 1998) and fractured by ~20 subsequent rifting episodes (Björnsson et al., 1979; Buck et al., 2006). The data quantity and quality and the presence of syn-kinematic deposits provide an unparalleled opportunity to consider a single fault system with D_{max}-L spanning two orders of magnitude.

KRAFLA FISSURES

The KFS lies within the Northern Volcanic Zone (NVZ) (Fig. 1A), one of four rift zones across Iceland (Sigmundsson, 2006). The NVZ extends north from the Vatnajökull icecap in central Iceland to the north coast where it meets the Tjörnes Fracture Zone (Einarsson, 1991), and encompasses a series of north-northeast–striking, left-stepping en echelon fissure swarms following the plate boundary (Einarsson, 2008). The NVZ includes five main volcanic systems: Askja, Kverkfjöll, Fremrinámar, Krafla, and Theistareykir (Fig. 1B). The KFS covers a 5–10-km-wide and 100-km-long region and transects the 200 ka active Krafla central volcano and caldera (Sæmundsson, 1991).

The KFS contains fractures that form a continuum from pure extensional fissures through to well-developed normal faults (Hjartardóttir et al., 2012). The main deformation region is largely confined to a central zone of fissures, commonly flanked by graben-bounding normal faults (Gudmundsson, 1984; Opheim and Gudmundsson, 1989). The resulting KFS forms a set of graben structures, with the central graben extending from south of Hverfjall through the central caldera toward the coast (Angelier et al., 1997) (Fig. 1) and the density of fault- and fissure-like fractures decreasing with distance from the central caldera (Hjartardóttir et al., 2012).

*E-mail: E.K.Bramham@leeds.ac.uk

CITATION: Bramham, E.K., et al., 2021, A new model for the growth of normal faults developed above pre-existing structures: Geology, v. 49, p. , https://doi.org/10.1130/G48290.1

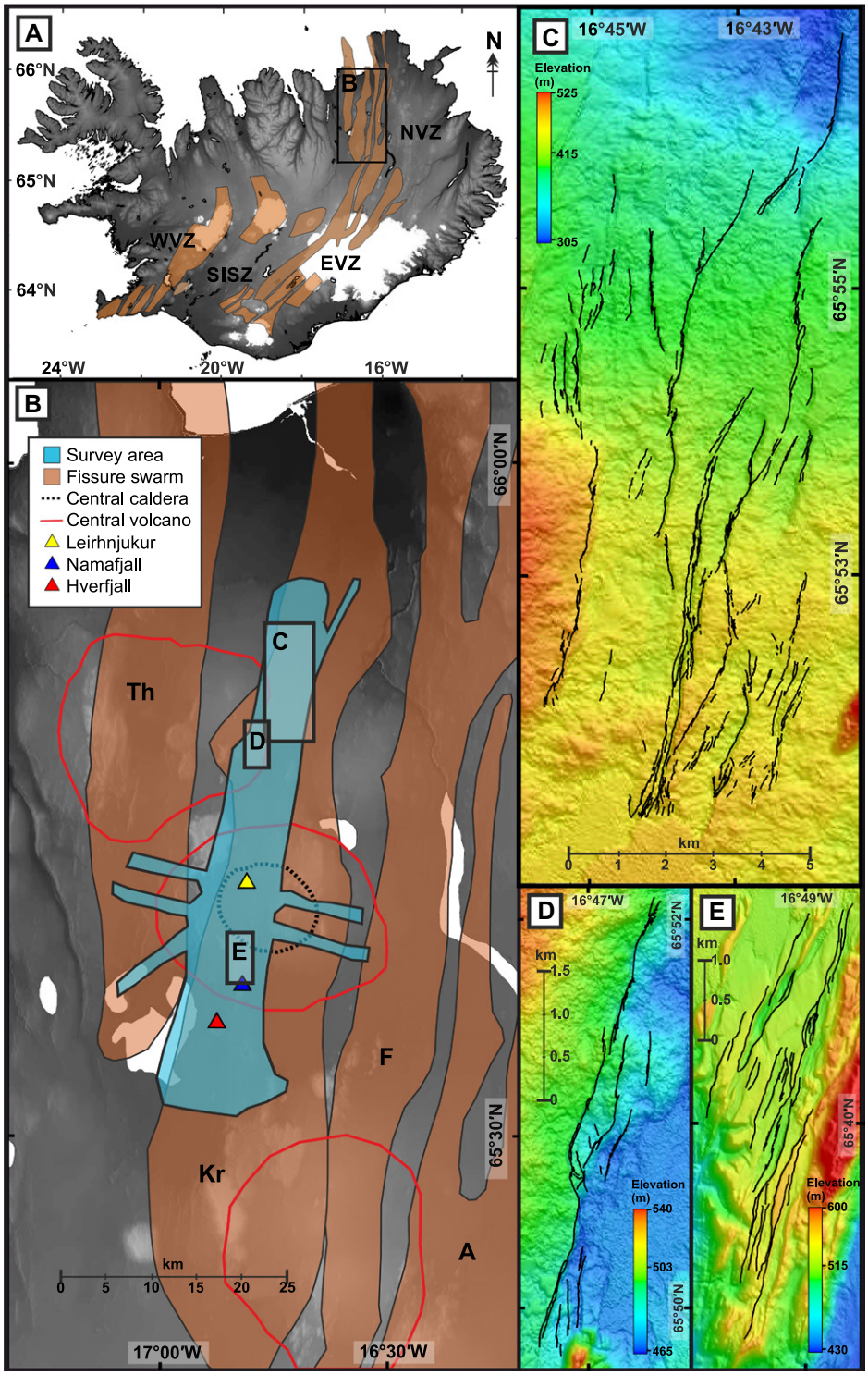

Figure 1. (A) Location map of Icelandic fissure swarms (orange) and main volcanic zones: WVZ—Western Volcanic Zone; SISZ—South Iceland seismic zone; EVZ—Eastern Volcanic Zone; NVZ—Northern Volcanic Zone. (B) Location of NVZ fissure swarms (Kr—Krafla; Th—Theistareykir; F—Fremrinámar; A—Askja), with the region covered by the lidar survey shown in blue. (C–E) Regions of the lidar digital elevation model used for fault measurements, with measured faults shown as black lines. Swarm outlines in A and B are from Einarsson and Sæmundsson (1987) and Hjartardóttir et al. (2016).

DATA AND METHODS

We used a series of airborne lidar surveys acquired on 7 August 2007 and 5 September 2008 by the UK Natural Environment Research Council (NERC) Airborne Research and Survey Facility (ARSF) Dornier aircraft; these surveys have an optimal resolution of ~0.5 m on the *x*- and *y*-axes and ~0.2 m on the *z*-axis, resulting in a high-resolution (0.5 m) digital elevation model (DEM) of the KFS. Following initial post-processing of the raw lidar point cloud data to *x*, *y*, and *z* coordinates by the Unit for Landscape Modelling (ULM), University of Cambridge (UK), we used a convergent interpolation algorithm (Haecker, 1992) to build the DEM. The DEM provides an unprecedented view of the topographic surface (Figs. 1C and 1D). Along-fault measurement intervals of 2–6 m (average ~4.8 m, decreasing to 2 m around fault tips and complex regions) are possible by using abrupt changes in surface expression to map hanging-wall and footwall cutoffs.

Given the subvertical nature of the faults in the KFS (Opheim and Gudmundsson, 1989), our compilation of vertical displacement profiles (the throw) allows us to compare faults across the study area, which includes fissure-like faults (here defined as primarily extensional fractures with significant segments of their vertical displacement profile at <1 m). We measured 775 faults with maximum displacement ranging from ~0.5 to 37 m and surface lengths from ~0.015 to 2 km. We extracted D_{max}/L for each measured fault and plotted them against the global population (Fig. 2A, bottom right inset), which reveals that there is a marked spread of data, particularly at lower displacements.

To investigate this wide distribution, we developed a quantitative approach for categorizing the fault profiles (detailed in Table 1) based on the percentage of fault profiles that have a vertical displacement >1 m. They range from category 1 fractures, which show no vertical displacement, to category 5 fractures, which show vertical displacements along their entire length (Fig. 2A, top inset). Category 5 fractures are subdivided into three subgroups (Table 1; Fig. 2B): fully displaced faults (5a, classical), exhibiting a single bell-shaped profile; faults with a flat-topped profile (5b, flat-top); and faults with local displacement minima (5c, linked; Fig. 2). We examined where within the range of the measured D_{max}/L data each category lies (Fig. 2A, main) and tested whether there is a relationship between fault geometry and a fault's location within the distribution.

DATA DISTRIBUTION AND INTERPRETATION

Category 1 and 2 fractures, representing fractures that are fissure-like (displacement <1 m) along 65% or more of their length, are preferentially distributed in the lower portion of the D_{max}/L plot (Fig. 2A). Noticeably, the distribution of fissure-like fractures has a well-defined upper limit in surface fault length, with only three fissure-like faults having lengths >400 m. Furthermore, with only four exceptions, all fractures with D_{max} <2 m are fissure-like (category 1 or 2), and these span lengths from ~15 to 400 m. D_{max}/L for fissure-like fractures spans nearly the full global range

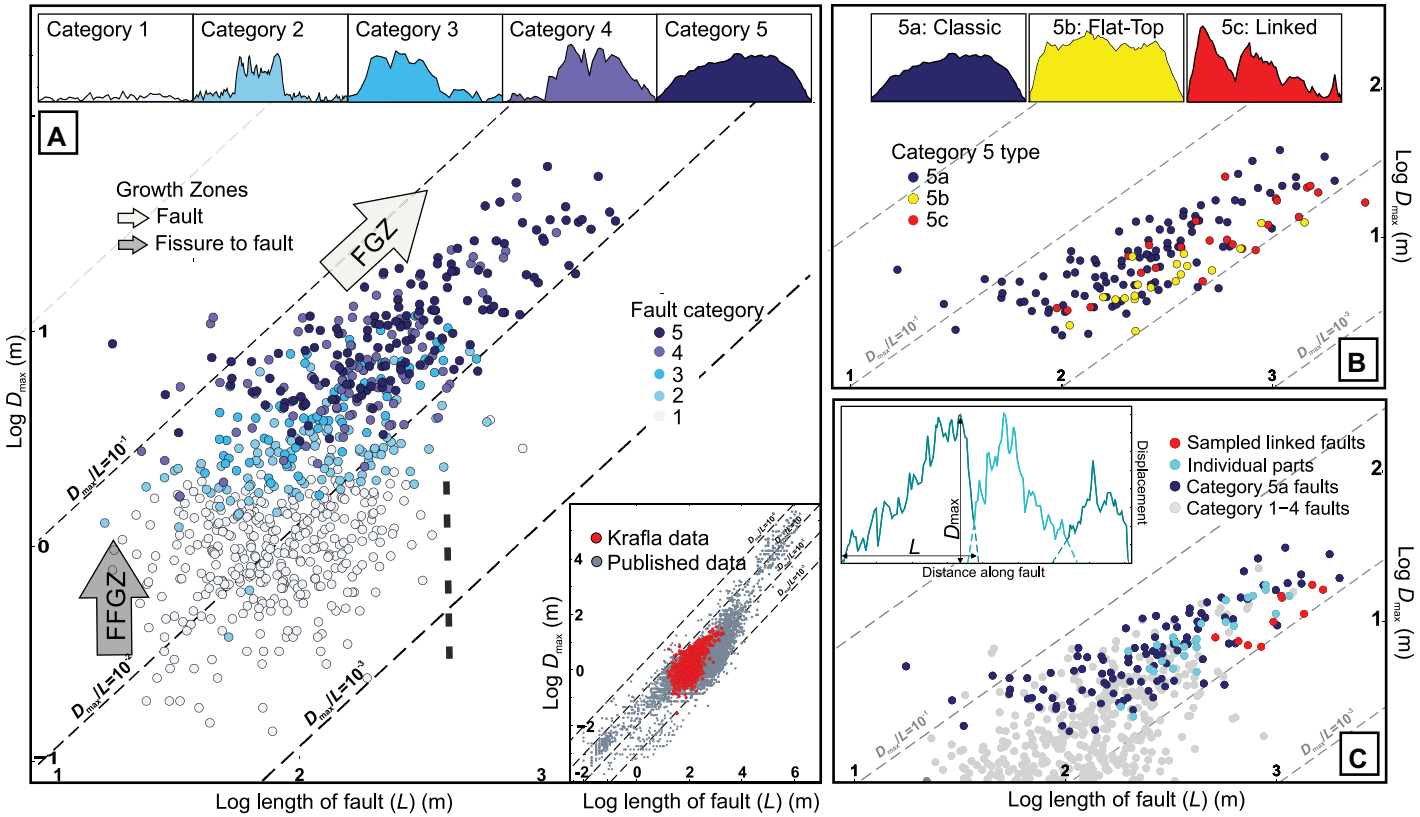

Figure 2. (A) Ratio of maximum vertical displacement to length (D_{max}/L) for Krafla faults (Iceland), categorized from 1 to 5 as described in Table 1, with example fault profiles shown in the top inset. The fracture to fault growth zone (FFGZ) and fault growth zone (FGZ) are represented by light and dark gray arrows, respectively, with dotted black line showing the approximate cutoff in surface fracture length in the FFGZ. Bottom inset: D_{max}/L data for Krafla faults (red) plotted alongside published D_{max}/L data as collated by Bailey et al. (2005). (B) Category 5a, 5b, and 5c faults, as described in Table 1, with example fault profiles in top inset. (C) Selected linked faults (red) and D_{max}/L of suggested component segments (turquoise) as estimated from extrapolating each linked section (example shown in inset shows a 5c profile with three component segments, extrapolated [dotted lines] to possible pre-linkage segment lengths).

($\sim 10^{-3}$ to 10^{-1}). Fractures that are predominantly fault-like (categories 4 and 5) plot with a much narrower range of D_{max}/L ($\sim 10^{-2}$ to 10^{-1}) and displacements >2 m for all but six faults. Category 3 fractures are both fissure- and fault-like, each for ~50% of their surface length, and form a transition in the D_{max}/L distribution between category 1 and 2 fissure-like and category 4 and 5 fault-like fractures.

This change in the characteristic shape of fracture displacement profiles supports a model of fault growth in which fractures evolve from being "fissure-like" to "fault-like" as they increase their vertical displacement, without changing their surface length. We refer to this region of the D_{max}/L plot as the fissure to fault growth zone (FFGZ; Fig. 2A). The correlation between length and displacement profile for "fault-like" fractures suggests fractures can only increase their length once displaced along >75% of their surface length. The absence of category 1–3 fractures with longer lengths implies that further displacement would be required before they could grow in length. We propose that this represents an evolution from the fissure-dominated FFGZ to the fault-dominated population referred to in the D_{max}/L plot as the fault growth zone (FGZ; Fig. 2A).

Fault-like fractures with >1 m displacement along >90% of their length have a range of shapes (5a, classic; 5b, flat-top; and 5c, linked; Fig. 2B). Category 5a faults are more likely to plot toward the uppermost limit of the ratio D_{max}/L in the global distribution, with category 5b and 5c faults showing lower D_{max} values for their lengths. Category 5c faults have *D-L* profiles that are consistent with them having formed by linkage of shorter segments. We have divided a subset of category 5c faults into their possible pre-linkage fault segment lengths using displacement minima (example shown in Fig. 2C, inset), and their D_{max}/L values measured. We observe that all the constituent faults lie within the category 5 region in the overall D_{max}/L distribution (Fig. 2C). This could imply that faults are more likely to grow by linkage when they are fault-like fractures. Alternatively, this relationship could be attributed to faults with larger vertical displacement slipping and propagating faster, and therefore linking more rapidly than smaller faults.

TABLE 1. PARAMETERS USED TO DEFINE FAULT CATEGORIES

Category	Proportion of fault with vertical displacement (%)	Minimum-maximum range used for %	Description
1	0	0–10	Minimal vertical displacement across the fault profile
2	~25	11–35	~25% of fault profile showing vertical displacement
3	~50	36–65	~50% of fault profile showing vertical displacement
4	~75	66–89	~75% of fault profile showing vertical displacement
5	100	90–100	Vertical displacement evident across the whole fault profile
5a	100		Category 5 fault with classical bell-shaped fault profile
5b	100		Category 5 fault with flattened fault profile
5c	100		Category 5 fault with linked fault profile

MODEL FOR FAULT GROWTH

By assuming that our analysis of a population of fissure- and fault-like fractures in the KFS represents a snapshot of *D-L* data of different stages of growth, we interpret that, in this location, faults form initially as fissures. The fissures then gradually increase their vertical

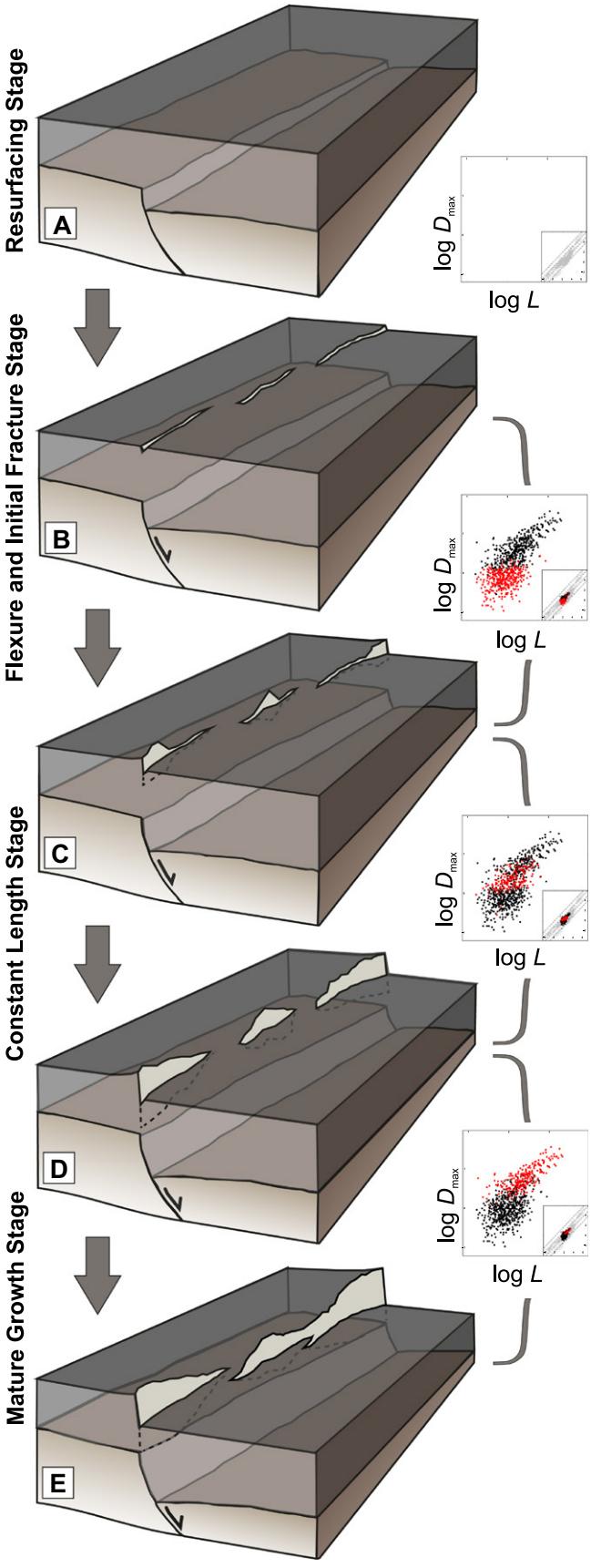

Figure 3. Model of fault growth showing initial stage of resurfacing (A); flexure and initial opening of extensional fracturing (B); growth in isolation from extensional fractures to faults through multiple slip events (C); fully formed fault moving into growth in isolation (D); and continued fault growth through dip and strike linkage of fully formed faults (E). Note that the growth stage shown in C represents the gradual development of a fully formed fault by the stage shown in D that would take many fault slip events to achieve a fully formed fault profile. D_{max}—maximum vertical displacement; L—length. D_{max}/L plots show the Krafla fault data (black) with the subset of fault data representing each stage of fault growth (red), and with inset showing these data alongside the global D_{max}/L data (gray).

displacement (FFGZ in Fig. 2) before entering a phase where both length and displacement increase (FGZ in Fig. 2). We propose that this pattern of fault growth is a result of the faults forming above pre-existing faults following resurfacing by the Storaviti lava flow (Fig. 3).

Collectively, our observations suggest four stages of fault growth. Initially there is a *resurfacing stage* (Fig. 3A), in which there is a geologically instantaneous episode of deposition of a homogenous package (in this case, the Storaviti lava flow) that buries the preexisting underlying faults. This is followed by the *flexure and initial fracture stage* (Fig. 3B), where slip on the underlying fault causes tensile bending stresses at the surface, resulting in horizontal opening of isolated fissures with minimal vertical displacements (<1 m). Subsequently, the fissures enter a *constant length stage* (Figs. 3C to 3D), with the faults propagating downward toward the underlying fault. The strike length of each fault that has displacement increases, as does the amount of total displacement, until the faults reach *D-L* profiles with displacements along >75% of the surface length (category 4 and 5 fractures). Faults then enter a *mature growth stage* (Figs. 3D to 3E) where they can grow by a combination of increasing both their displacement and length in isolation and by increasing their length by strike linkage and dip linkage (e.g., Rykkelid and Fossen, 2002) to increase their displacement accumulation. In this final stage, data distribution tends toward the higher boundary of the ratio D_{max}/L in the published global distribution. The process would be repeated following the next phase of resurfacing. We suggest that fault segments can remain unconnected from one another and from the underlying structure for most of their evolution, but can form dip linkage with the underlying fault in the final stages of the growth model. An important consideration is the rheology of basalt, where columnar jointing lends itself to accommodating flexure through fissuring. In contrast, weaker or unlithified sedimentary successions could be more likely to accommodate flexure through folding (e.g., Childs et al., 2017) in the flexure and initial fracture stage.

IMPLICATIONS AND CONCLUSIONS

The wide distribution of global D_{max}/L data in previous compilations has been attributed to differences in tectonic setting, lithology, or maturity of the individual systems (Cartwright et al., 1995). Our results demonstrate that D_{max}/L data, even in a very well-constrained setting, have a wide natural variability. The combination of data resolution and syn-kinematic evolution involving both radial tip propagation and the linkage of initially isolated segments leads to this wide distribution.

Although our findings are most directly applicable to magmatic divergent plate boundaries, including mid-ocean ridges and subaerial magmatic systems such as those in Iceland or Ethiopia, they have wider implications for how *D-L* relationships are interpreted. *D-L* relationships have been widely used to estimate regional strain and to discriminate strain zones (Soliva and Schulz, 2008; Polun et al., 2018). Our results

suggest that care must be taken when applying surface fault *D-L* relationships from topographic data to predict deeper fault-controlled mechanisms, e.g., when comparing surface fault relationships in slow- and fast-spreading mid-ocean ridges (Shaw and Lin, 1996; Bohnenstiehl and Kleinrock, 2000) where rates of resurfacing relative to tectonic strain may not be comparable. Application of our model could be critical in informing subsurface geological models that are commonly reliant on surface fault data, e.g., hydrothermal and geothermal systems in which underlying faults play a key role in controlling fluid flow (Hayman and Karson, 2007).

Our observations are applicable beyond divergent magmatic plate boundaries. Seismic hazard mapping in magmatic and sedimentary systems commonly relies upon surface fault expression to predict deeper fault patterns (Scholz and Gupta, 2000), yet we show that this may be a poor predictor of underlying faults where resurfacing occurs. On longer time scales, hybrid models have been applied to explain cumulative slip in sedimentary basin evolution (Rotevatn et al., 2019). Our model suggests such processes are present over the much shorter time scale of the seismic slip–syn-kinematic deposition cycle. Furthermore, our new model for fault growth can be applied to seismic reflection data, particularly aspects of fault growth such as early-stage evolution of fault zones that are not readily detected in conventional data sets (Hayman and Karson, 2007; Baudon and Cartwright, 2008; Welch et al., 2009).

ACKNOWLEDGEMENTS

We thank the UK Natural Environment Research Council (NERC) for supporting this research (grant NE/E007414/1 and studentship for Bramham), the NERC Airborne Research and Survey Facility (ARSF) for the lidar acquisition, Schlumberger (Gatwick, UK) for providing Petrel software, Freysteinn Sigmundsson and Asta Rut Hjartardóttir for support in Iceland, and John Walsh, Páll Einarsson, Chris Jackson, and Giovanni Camanni for their constructive reviews. The NERC Centre for the Observation and Modelling of Earthquakes, Volcanoes and Tectonics (COMET) is a partnership between UK universities and the British Geological Survey.

REFERENCES CITED

Angelier, J., Bergerat, F., Dauteuil, O., and Villemin, T., 1997, Effective tension-shear relationships in extensional fissure swarms, axial rift zone of northeastern Iceland: Journal of Structural Geology, v. 19, p. 673–685, https://doi.org/10.1016/S0191-8141(96)00106-X.

Bailey, W.R., Walsh, J.J., and Manzocchi, T., 2005, Fault populations, strain distribution and basement fault reactivation in the East Pennines Coalfield, UK: Journal of Structural Geology, v. 27, p. 913–928, https://doi.org/10.1016/j.jsg.2004.10.014.

Baudon, C., and Cartwright, J., 2008, The kinematics of reactivation of normal faults using high resolution throw mapping: Journal of Structural Geology, v. 30, p. 1072–1084, https://doi.org/10.1016/j.jsg.2008.04.008.

Björnsson, A., Johnsen, G., Sigurdsson, S., Thorbergsson, G., and Tryggvason, E., 1979, Rifting of the plate boundary in north Iceland 1975–1978: Journal of Geophysical Research, v. 84, p. 3029–3038, https://doi.org/10.1029/JB084iB06p03029.

Bohnenstiehl, D.R., and Kleinrock, M.C., 2000, Evidence for spreading-rate dependence in the displacement-length ratios of abyssal hill faults at mid-ocean ridges: Geology, v. 28, p. 395–398, https://doi.org/10.1130/0091-7613(2000)28<395:EFSDIT>2.0.CO;2.

Buck, W.R., Einarsson, P., and Brandsdóttir, B., 2006, Tectonic stress and magma chamber size as controls on dike propagation: Constraints from the 1975–1984 Krafla rifting episode: Journal of Geophysical Research, v. 111, B12404, https://doi.org/10.1029/2005JB003879.

Cartwright, J.A., Trudgill, B.D., and Mansfield, C.S., 1995, Fault growth by segment linkage: An explanation for scatter in maximum displacement and trace length data from the Canyonlands Grabens of SE Utah: Journal of Structural Geology, v. 17, p. 1319–1326, https://doi.org/10.1016/0191-8141(95)00033-A.

Childs, C., Manzocchi, T., Nicol, A., Walsh, J.J., Soden, A.M., Conneally, J.C., and Delogkos, E., 2017, The relationship between normal drag, relay ramp aspect ratio and fault zone structure, *in* Childs, C., et al., eds., The Geometry and Growth of Normal Faults: Geological Society [London] Special Publication 439, p. 355–372, https://doi.org/10.1144/SP439.16.

Cowie, P.A., and Scholz, C.H., 1992, Displacement-length scaling relationship for faults: Data synthesis and discussion: Journal of Structural Geology, v. 14, p. 1149–1156, https://doi.org/10.1016/0191-8141(92)90066-6.

Einarsson, P., 1991, Earthquakes and present-day tectonism in Iceland: Tectonophysics, v. 189, p. 261–279, https://doi.org/10.1016/0040-1951(91)90501-I.

Einarsson, P., 2008, Plate boundaries, rifts and transforms in Iceland: Jökull, v. 58, p. 35–58.

Einarsson, P., and Sæmundsson, K., 1987, Earthquake epicenters 1982–1985 and volcanic systems in Iceland, *in* Sigfusson, Th., ed., I hlutarins edli: Festschrift for Thorbjorn Sigurgeirsson: Reykjavik, Menningarsjodur, one sheet, scale 1:750000.

Gudmundsson, A., 1984, Tectonic aspects of dykes in northwestern Iceland: Jökull, v. 34, p. 81–96.

Gupta, S., Cowie, P.A., Dawers, N.H., and Underhill, J.R., 1998, A mechanism to explain rift-basin subsidence and stratigraphic patterns through fault-array evolution: Geology, v. 26, p. 595–598, https://doi.org/10.1130/0091-7613(1998)026<0595:AMTERB>2.3.CO;2.

Haecker, M.A., 1992, Convergent gridding: A new approach to surface reconstruction: Geobyte, v. 7, p. 48–53.

Hayman, N.W., and Karson, J.A., 2007, Faults and damage zones in fast-spread crust exposed on the north wall of the Hess Deep Rift: Conduits and seals in seafloor hydrothermal systems: Geochemistry Geophysics Geosystems, v. 8, Q10002, https://doi.org/10.1029/2007GC001623.

Hjartardóttir, Á.R., Einarsson, P., Bramham, E., and Wright, T.J., 2012, The Krafla fissure swarm, Iceland, and its formation by rifting events: Bulletin of Volcanology, v. 74, p. 2139–2153, https://doi.org/10.1007/s00445-012-0659-0.

Hjartardóttir, Á.R., Einarsson, P., Magnúsdóttir, S., Björnsdóttir, Þ., and Brandsdóttir, B., 2016, Fracture systems of the Northern Volcanic Rift Zone, Iceland: An onshore part of the Mid-Atlantic plate boundary, *in* Wright, T.J., et al., eds., Magmatic Rifting and Active Volcanism: Geological Society [London] Special Publication 420, p. 297–314, https://doi.org/10.1144/SP420.1 .

Jóhannesson, H., and Sæmundsson, K., 1998, Geological map of Iceland: Bedrock geology: Reykjavik, Icelandic Institute of Natural History and Iceland Geodetic Survey, scale 1:500,000.

Opheim, J.A., and Gudmundsson, A., 1989, Formation and geometry of fractures, and related volcanism, of the Krafla fissure swarm, northeast Iceland: Geological Society of America Bulletin, v. 101, p. 1608–1622, https://doi.org/10.1130/0016-7606(1989)101<1608:FAGOFA>2.3.CO;2.

Peacock, D.C.P., and Sanderson, D.J., 1991, Displacements, segment linkage and relay ramps in normal fault zones: Journal of Structural Geology, v. 13, p. 721–733, https://doi.org/10.1016/0191-8141(91)90033-F.

Polun, S.G., Gomez, F., and Tesfaye, S., 2018, Scaling properties of normal faults in the central Afar, Ethiopia and Djibouti: Implications for strain partitioning during the final stages of continental breakup: Journal of Structural Geology, v. 115, p. 178–189, https://doi.org/10.1016/j.jsg.2018.07.018.

Rotevatn, A., Jackson, C.A.-L., Tvedt, A.B.M., Bell, R.E., and Blækkan, I., 2019, How do normal faults grow?: Journal of Structural Geology, v. 125, p. 174–184, https://doi.org/10.1016/j.jsg.2018.08.005.

Rykkelid, E., and Fossen, H., 2002, Layer rotation around vertical fault overlap zones: Observations from seismic data, field examples, and physical experiments: Marine and Petroleum Geology, v. 19, p. 181–192, https://doi.org/10.1016/S0264-8172(02)00007-7.

Sæmundsson, K., 1991, Geology of the Krafla system, *in* Garðarsson, A., and Einarsson, Á., eds., Náttúra Mývatns: Reykjavik, Hid Islenska Natturufraedifelag, p. 24–95 (in Icelandic).

Scholz, C.H., and Gupta, A., 2000, Fault interactions and seismic hazard: Journal of Geodynamics, v. 29, p. 459–467, https://doi.org/10.1016/S0264-3707(99)00040-X.

Schultz, R.A., and Fossen, H., 2002, Displacement-length scaling in three dimensions: The importance of aspect ratio and application to deformation bands: Journal of Structural Geology, v. 24, p. 1389–1411, https://doi.org/10.1016/S0191-8141(01)00146-8.

Shaw, W.J., and Lin, J., 1996, Models of ocean ridge lithospheric deformation: Dependence on crustal thickness, spreading rate, and segmentation: Journal of Geophysical Research, v. 101, p. 17,977–17,993, https://doi.org/10.1029/96JB00949.

Sigmundsson, F., 2006, Iceland Geodynamics: Crustal Deformation and divergent Plate Tectonics: Chichester, UK, Praxis Publishing, Springer Verlag, 209 p.

Soliva, R., and Schulz, R.A., 2008, Distributed and localized faulting in extensional settings: Insight from the north Ethiopian Rift–Afar transition area: Tectonics, v. 27, TC2003, https://doi.org/10.1029/2007TC002148.

Walsh, J.J., and Watterson, J., 1988, Analysis of the relationship between displacements and dimensions of faults: Journal of Structural Geology, v. 10, p. 239–247, https://doi.org/10.1016/0191-8141(88)90057-0.

Walsh, J.J., Nicol, A., and Childs, C., 2002, An alternative model for the growth of faults: Journal of Structural Geology, v. 24, p. 1669–1675, https://doi.org/10.1016/S0191-8141(01)00165-1.

Welch, M.J., Knipe, R.J., Souque, C., and Davies, R.K., 2009, A Quadshear kinematic model for folding and clay smear development in fault zones: Tectonophysics, v. 471, p. 186–202, https://doi.org/10.1016/j.tecto.2009.02.008.

Printed in USA